

# Mediation mechanism of tyrosine 185 on the retinal isomerization equilibrium and the proton release channel in the seven-transmembrane receptor bacteriorhodopsin\*

Xiaoyan Ding<sup>1</sup>, Honglei Wang<sup>2</sup>, Bo Peng<sup>1</sup>, Haolin Cui<sup>1</sup>, Yujiao Gao<sup>1</sup>, Dinu Iuga<sup>3</sup>, Peter J. Judge<sup>4</sup>, Guohui Li<sup>2,†</sup>, Anthony Watts<sup>4,†</sup> and Xin Zhao<sup>1,†</sup>

<sup>1</sup>Shanghai Key Laboratory of Magnetic Resonance, Department of Physics, East China Normal University, Shanghai 200062, P.R. China

<sup>2</sup>State Key Laboratory of Molecular Reaction Dynamics, Dalian Institute of Chemical Physics, Chinese Academy of Sciences, Liaoning 116023, P. R. China

<sup>3</sup>The UK 850 MHz Solid-State NMR Facility, Department of Physics, University of Warwick, Coventry CV4 7AL, UK

<sup>4</sup>Biomembrane Structure Unit, Department of Biochemistry, University of Oxford, South Parks Road, Oxford OX1 3QU, UK

<sup>†</sup>Corresponding authors:

Shanghai Key Laboratory of Magnetic Resonance, Department of Physics; East China Normal University, Shanghai 200062, P. R. China. Tel.: +86-21-62234329; Fax: +86-21-62234329; Email: xzhao@phy.ecnu.edu.cn

Department of Biochemistry, University of Oxford, South Parks Road, Oxford OX1 3QU, UK.

Tel.: +44-1865-613219; Fax: +44-1865-613201;

Email: anthony.watts@bioch.ox.ac.uk

State Key Laboratory of Molecular Reaction Dynamics, Dalian Institute of Chemical Physics,

Chinese Academy of Sciences, Liaoning 116023, P. R. China. Tel.: +86-411-84379593; Fax:

+86-411-84379593; Email: ghli@dicp.ac.cn

\*This article contains Supplementary material.

## **ABSTRACT**

Electrostatic coupling leading to conformational changes in proteins is challenging to demonstrate directly, it requires that both the local, discrete electronic details and dynamic information relevant to the functional descriptions are probed. Here, as a novel study to address this challenge, the roles of an aromatic residue in influencing the functional conformational changes of a membrane receptor in its natural membrane environment are reported. Previously intractable discrete electronic details have been obtained using 2D solid-state NMR of specifically labelled receptor, reinforced with molecular dynamic simulations, mutational analysis and functional assays, supported by and compared with rigid-atom crystal structural models. Hydrogen bonding and hydrophobic interactions are identified as the mechanistic origin for direct electromechanical coupling to the dynamics of conformational changes within the receptor.

## **KEYWORDS**

Electrostatic coupling, functional conformational change, aromatic residue, mutational analysis and functional assays, solid-state NMR

## 1. Introduction

Bacteriorhodopsin (bR), a member of the microbial rhodopsin family of seven-transmembrane (TM) receptors, functions as a light-driven proton pump for light energy capture in *Halobacterium salinarum* [1]. The retinal (Ret) chromophore is covalently bound to Lys216 on helix G to form a protonated Schiff base (SB) [2]. In the dark, two Ret isomers, 13-cis, 15-syn Ret (bR<sub>cis</sub>) and all-trans, 15-anti Ret (bR<sub>trans</sub>), are thermally interconvertible with a molar ratio close to 1:1 [3-6]. Conversion of the cis isomer to the all-trans configuration under illumination is known as light adaptation [6, 7]. Absorption of a photon causes photoisomerization of the chromophore from the all-trans to the 13-cis, 15-anti configuration and triggers a series of structural rearrangements in the protein that initiates the vectorial translocation of a proton out of the cell [8].

The *cis-trans* thermal equilibrium of the Ret chromophore occurs in many bacterial rhodopsins in their native membrane, including bR [3], Neurospora Rhodopsin [9], Proteorhodopsin [10], Anabaena Sensory Rhodopsin [11], Channelrhodopsin-2 [12], Halorhodopsin [13], Xanthorhodopsin [14], Archaerhodopsin I-III [15-17]. However, the mechanism by which this equilibrium is maintained is not well described, and the direct demonstration of electrostatic coupling leading to conformational changes within proteins that explore multiple equilibria of states, is still challenging.

In bR, there are 26 amino acid residues contributing to the proton translocation channel in five helices, and 21 residues surround the Ret to form a binding pocket by all seven helices. Among them, 10 residues located in the middle of the proton translocation channel are also part of the Ret binding pocket [18]. Methionine 145

(M145), one of the residues contributing to the binding pocket on helix E, was the first residue identified to affect the *cis-trans* thermal equilibrium of the Ret chromophore in the dark [15]. The M145F mutation was shown to reduce the motional freedom of the tryptophan 182 in contact with the C13 methyl group of the Ret and to further destabilize the L state of bR [19]. On the other hand, tyrosine 185 (Y185), a binding site residue, was reported to play an important role in stabilizing the pentagonal hydrogen-bond network on the extracellular side of the retinal-lysine216 Schiff base (SB), and involved in the reprotonation of the SB during the early stages of the photocycle [20-23]. Furthermore, a  $^{13}\text{C}$  solid-state NMR (ssNMR) study of  $[4^1\text{-}^{13}\text{C}]$ -labelled tyrosine showed that the 11 tyrosine residues are protonated over a wide pH range from 2 to 12 in dark-adapted bR [24]. Similarly, two different but co-existing conformations of Y185, based on a 4.3 ppm splitting of the  $^{13}\text{CO}$  chemical shift of Y185, were observed [25, 26]. The thermal conversion between the all-*trans* and 13-*cis* configuration of Ret in the dark-adapted purple membrane was considered to be the cause of the Y185 conformational change [25]. However, the crystal and solution NMR structures of bR<sub>trans</sub> and bR<sub>cis</sub> showed no displacements of Y185 during dark-light adaptation [27-29]. Therefore, the roles of Y185 in the bR photoreaction mechanism requires further clarification with respect to the thermal isomerization equilibrium of the Ret chromophore, and conformational modulation of proton release during the bR photocycle.

In this study, the roles of Y185 in influencing the functional conformational changes of bR in its natural membrane environment are reported. Two-dimensional (2D) magic-angle spinning ssNMR of specifically labeled bR, reinforced with light-induced transient absorption measurements, molecular dynamics (MD) simulations

and site-directed mutagenesis was used to examine how Y185 interacts with the Ret chromophore and modulates the proton release channel through aspartic acid 212 (D212) in its natural membrane environment. We first show that Y185 both maintains the *cis-trans* isomerization thermal equilibrium of the Ret chromophore, and retains aspartic acid 212 in a favorable conformation through a hydrogen bond to produce a cascade of conformational changes associated with photoreactions with the appropriate lifetime. Removal of the phenolic hydroxyl group in the Y185F mutant shifts the *cis-trans* isomerization thermal equilibrium to a bR<sub>cis</sub>-dominated state and causes a weakening of the M state, loss of the O state and elongation of the proton pump cycle time.

## **2. Material and methods**

### **2.1 Synthesis of <sup>13</sup>C-labelled all-*trans*-retinal**

[10, 11-<sup>13</sup>C<sub>2</sub>]-, [14, 15-<sup>13</sup>C<sub>2</sub>]- and [10, 11, 14, 15-<sup>13</sup>C<sub>4</sub>]-labelled Ret molecules were synthesized by the standard method developed by Groesbeek and Lugtenburg [30]. The <sup>13</sup>C-labelled all-*trans*-Ret was purified by preparative HPLC using a 10 μm Luster Silica gel column (250×10.0mm). Purity of the <sup>13</sup>C-labelled all-*trans*-Ret was examined by <sup>1</sup>H NMR on a 500 MHz spectrometer, and the isotope enrichment was better than 99%. The synthetic routes of the <sup>13</sup>C-labelled Ret are illustrated in Figure S1 in the Supplementary material.

### **2.2 Protein sample preparations**

Wild-type bR (WT-bR) purple membranes and Y185F mutant (Y185F-bR) were cultured and isolated by using either *H. salinarum* strain R1M1 or *H. salinarum* strain

L33, and a sucrose gradient with concentrations of 35%, 43% and 60% (w/w) was used for purification of the purple membranes, according to previously described standard procedures [31]. The concentration of the purified bR was determined based on the absorption maximum at 568 nm using an extinction coefficient of  $62700 \pm 700 \text{ M}^{-1}\text{cm}^{-1}$  [32].  $^{13}\text{C}$ - and  $^{15}\text{N}$ -labelled wild-type and Y185F mutant purple membranes were prepared by growing R1M1 and L33 in the synthetic media separately, in which the unlabelled tyrosine was replaced by the isotope-labelled one [33].

### **2.3 Incorporation of $^{13}\text{C}$ -labelled all-*trans*-Ret into the bR purple membrane**

$^{13}\text{C}$ -labelled-all-*trans*-Ret was incorporated into the bR purple membrane via bleaching and regeneration as previously described [34, 35]. Briefly, the bR purple membrane was first completely bleached by illumination of the suspension in 50 ml of 0.5 M hydroxylamine at pH 7.0 for 3 hours with a 550 nm cutoff filter; the bleached sample was then washed three times with 10 mM HEPES buffer (pH 7.0), and the  $^{13}\text{C}$ -labelled-all-*trans*-Ret (1.2 molar ratio excess) was slowly added in the dark with vigorous shaking at room temperature. Finally, the mixture was incubated at 4 °C in the dark for 24 hours and then washed five times with 2% BSA to remove the unincorporated free Ret. The incorporation yield was approximately 80%.

### **2.4 UV-vis spectroscopy**

UV-vis spectra were recorded using a T6 New Century spectrophotometer. (Beijing Purkinje General Co. Ltd). The bR purple membrane was kept in the dark at room temperature for 2 hours to ensure a fully dark-adapted form. The dark-

adapted UV-vis measurement was then taken in the dark. The samples were then illuminated for 5 minutes to convert the dark-adapted form into the light-adapted form, and the light-adapted UV-vis spectrum was then recorded.

## **2.5 Light-induced transient absorption change spectroscopy**

The proton pumping activities of bR were monitored through a light-induced absorption change using a pH-sensitive dye, pyranine, on a homemade apparatus as described previously [36]. The net proton pumping activity was determined by taking the absorbance difference at 456 nm before and after adding the dye. The kinetics of the M state, O state and recovery trajectory to the ground state were monitored at 410 nm, 660 nm and 570 nm, respectively. All experiments were carried out by using a photoflash with the half-bandwidth less than 1 ms for excitation; the measurements were performed at room temperature.

## **2.6 Solid-state NMR experiments**

All solid-state NMR measurements were performed on either a Bruker 600 MHz Avance III wide bore spectrometer at  $-25\pm 1^\circ\text{C}$  or on a Bruker 850 MHz Avance III wide bore spectrometer at  $-65\pm 1^\circ\text{C}$ . A 3.2 mm or a 4.0 mm probe configured either in a double resonance or a triple resonance mode was used with a MAS spinning frequency of 8-16 kHz for different experiments. In all experiments, a ramped cross-polarization (CP) [37] with a 90%–100% linear gradient was used at a radio frequency (rf) field of 50 kHz on the proton channel. Typical 90° rf pulse lengths of 3.8  $\mu\text{s}$  for  $^{13}\text{C}$  and 2.7  $\mu\text{s}$  for  $^1\text{H}$  channels and the two-pulse phase modulation (TPPM) [38] with a pulse width of 5.5-6  $\mu\text{s}$  for proton decoupling were used throughout the experiments.



A recycle delay of 3 s was set for all the experiments. Detailed experimental setups for different 2D experiments are shown in the Supplementary material.

## **2.7 Molecular dynamic simulations**

The POPC membrane was treated using the General Amber force field model for lipids [39]. The system contains 239 phospholipid molecules, with each phospholipid molecule consisting of 134 atoms. Asp96, Asp115, Glu204 and the SB in the inactive state and Asp85, Asp96 and Asp115 in the M state were protonated. To parameterize bR, the electrostatic potentials of both the ground and M states were calculated using Gaussian 09 [40] with the 6-31G\* basis set and then used to obtain the restrained electrostatic potential (RESP) [41] fit of retinal-Lys Schiff base. Dihedral torsion potential parameters of both protonated and neutral Ret were achieved based on the work of Tajkhorshid [42], except for the parameter C12=C13-C14=C15, which was achieved based on the work of Hayashi et al. [43]. MD simulations were performed using the Gromacs dynamics software package [44], with the total simulation time set to 1  $\mu$ s and the integration step set to 2 fs (leap-frog algorithm). The Nose-Hoover thermostat method [45] and Parrinello-Rahman method [46] were employed to maintain a constant temperature (300 K) and pressure (1 bar). The particle mesh Ewald (PME) method [47] was applied to treat the long-range Columbic interactions.

## **3. Results**

### **3.1 Activity assessments of the reconstituted $^{13}\text{C}$ -all-trans-Ret bR purple membrane**

Reconstituted bR was shown to be functionally active through UV-vis spectroscopy and light-induced transient absorption measurements, as shown in Figure 1. The absorption maximum at 568 nm was observed for the wild-type bR purple membranes before bleaching (A1), disappeared after bleaching (A2), and was restored after reconstitution with the  $^{13}\text{C}$ -all-*trans*-Ret (A3). Similar observations were obtained for the formation and decay of the M state (B1-B3) and the proton pumping behaviour (C1-C3). Clearly, bR function was resumed completely after the reconstitution of the labelled Ret.

### **3.2 Chemical shift assignments of $^{13}\text{C}_9$ -Y185 and [10, 11, 14, 15- $^{13}\text{C}_4$ ]-Ret in bR purple membrane**

Of the 11 tyrosine residues in bR, most are located in helices. Y185 in helix 6 and Y57 in helix 2 are both associated with the SB-D85-D212-R82 hydrogen bond network within the Ret binding site [48], and thus any change in the  $^{13}\text{C}$  chemical shifts of Y185 can be compared with Y57. Furthermore, Y185-P186 on helix F and Y57-L58 on helix B are the unique tyrosine-proline and tyrosine-leucine pairs in bR, and the  $^{13}\text{CO}$  signals of Y185 and Y57 can be uniquely extracted from the 11 tyrosine residues through a 2D N-C filtration experiment using the double cross-polarization scheme (DCP) [49]. Figure 2 shows the 2D NCOCX spectra of bR with uniform  $^{13}\text{C}$ - and  $^{15}\text{N}$ -labelled tyrosine and  $^{15}\text{N}$ -labelled leucine and proline. Two intense contours arise at 176.1ppm/121.4ppm and 174.2 ppm/133.4 ppm in this spin-pair filtration experiment, which can be assigned to  $\text{Y57}^{13}\text{C}=\text{O}/\text{L58}^{15}\text{N}$  and  $\text{Y185}^{13}\text{C}=\text{O}/\text{P186}^{15}\text{N}$ , respectively. This assignment is attributed to the unique structural feature of proline whose  $^{15}\text{N}$  signal is well separated from other residues in bR, and similar chemical shift values

have been reported from solution NMR of detergent-solubilized bR, and ssNMR of Proteorhodopsin and Anabaena Sensory Rhodopsin of the same residues [28, 50, 51]. The chemical shifts of  $^{13}\text{C}\alpha$ ,  $^{13}\text{C}\beta$ ,  $^{13}\text{C}\epsilon$  and  $^{13}\text{C}\zeta$  of Y185 are clearly resolved by the NCOCX correlation experiment, and a clear double peak for  $^{13}\text{C}\alpha$  and  $^{13}\text{C}\beta$ , and a broader peak feature for  $^{13}\text{C}\epsilon$  and  $^{13}\text{C}\zeta$  of Y57 are observed in the spectra, indicating that Y57 may exist in more than one conformation in dark-adapted bR. Another possibility is that the  $^{13}\text{C}$ -labelled tyrosine residues may be metabolised into another amino acids *in vivo*, thus forming a  $^{13}\text{C}$ - $^{15}\text{N}$  pair with the adjacent leucine residue during ribosomal protein synthesis.

Combining the 2D NCOCX experiment with the 2D proton-driven spin diffusion (PDSD) [52] experiment (Figure 3), the carbon chemical shifts of Y185 and Y57 can be resolved for most of the sites listed in Table 1. Large shifts are observed, in particular for the CO and C $\zeta$  sites. The 2 ppm up-field shift for CO of Y185 may be attributed to the distorted helical structure of helix F pivoted at P186, which is termed as “Proline effect”. The 2 ppm down-field shift for C $\zeta$  indicates that a special interaction may exist between Y185 and Ret because Y185 is part of the Ret binding site. For C $\epsilon$ , Y185 shows a 1.0 ppm up-field shift relative to Y57, indicating a more hydrophobic local environment. C $\gamma$  and C $\delta$  of Y185 occur at 128.4 ppm and 132.8 ppm, respectively. However, C $\gamma$  and C $\delta$  of Y57 are difficult to resolve due to the uncertainty in the corresponding split C $\beta$  peak. The chemical shift assignments of the four sites labelled in Ret in the bR purple membrane were obtained through a 2D  $^{13}\text{C}$ - $^{13}\text{C}$  DQ-SQ correlation experiment on the [10, 11, 14, 15- $^{13}\text{C}_4$ ]-labelled-Ret-bR (Figure 4; Table 2). A notable down-field shift of C15 in bR<sub>cis</sub> and a larger peak separation between C15 and C14 in bR<sub>cis</sub> than in bR<sub>trans</sub> was observed, indicating that the C15–C14 bond may

be more twisted in  $bR_{cis}$  or that additional interactions occur at this site, since the charge accumulation on the N–H bond of the SB is likely to be similar in both the  $bR_{cis}$  and  $bR_{trans}$ . An observed smaller separation between C11 and C10 may indicate that the C11–C10 bond remains relatively flat and less affected by the isomerization in both  $bR_{cis}$  and  $bR_{trans}$ . Similar chemical shift values have been reported for singly C11-, C14- and C15-labelled Ret in dark-adapted bR purple membrane [53, 54].

### 3.3 H–C–C–H torsion angles and C–H bond lengths of the Ret chromophore in the dark-adapted bR purple membrane

Local distortion and configurational dynamics along the Ret polyene chain in  $bR_{cis}$  and  $bR_{trans}$  are best explored by ssNMR based on H–C–C–H torsion angles and C–H bond length measurements. Experimental results and simulations of H–C10–C11–H and H–C14–C15–H torsion angles and C10–H, C11–H C14–H and C15–H bond lengths in dark-adapted bR were measured (Figures S3 and S4). The estimated values of the different torsion angles and bond lengths are summarized in Tables S1 and S2. Our results show that the C10–C11 bond is clearly flatter than the C14–C15 bond in both  $bR_{cis}$  and  $bR_{trans}$ . The distortion of the C14–C15 bond in  $bR_{cis}$  is much more severe than that in the  $bR_{trans}$  configuration. The librational motion of all the C–H bonds remains similar, except for the C15–H bond in the  $bR_{cis}$  configuration that shows unusual rigidity. This feature may indicate that the more populated  $bR_{cis}$  in the thermal equilibrium compared with  $bR_{trans}$  in the dark, is stabilized by an interaction at the C15 site, which is likely to be induced by the electrostatic interaction with the phenolic hydroxyl group of Y185, as indicated by the further down-field shift of the

$^{13}\text{C}\zeta$  chemical shift of Y185 in  $\text{bR}_{cis}$ . A similar result was reported for the H–C14–C15–H torsion angle in the light-adapted bR membrane [54].

### 3.4 Coupling of Y185 with the Ret chromophore in the dark-adapted bR purple membranes

The contacts between Y185 and the Ret chromophore in the dark-adapted bR have been investigated by 2D  $^{13}\text{C}$ – $^{13}\text{C}$  PDSD correlation experiment. According to its crystal structure [48], Y185 is the only tyrosine residue out of the 11 that is within the potential NMR-observable distance to the Ret chromophore through a longer mixing time (500 ms) by spin diffusion in the PDSD experiment [55]. Figure 5 shows the 2D  $^{13}\text{C}$ – $^{13}\text{C}$  PDSD correlation spectra on the  $[\text{U-}^{13}\text{C}_9, ^{15}\text{N}]$ -Y-labelled bR purple membrane incorporated with  $[10, 11, 14, 15\text{-}^{13}\text{C}_4]$ -Ret. Y185C $\epsilon$ -RetC14 and Y185C $\zeta$ -RetC14 cross-peaks are observed in both  $\text{bR}_{cis}$  and  $\text{bR}_{trans}$ . As indicated by the NCOCX experiments, Y185 exhibits a single configuration in the dark-adapted bR purple membrane; this stable configuration may be attributed to the hydrogen bonding of the phenolic hydroxyl hydrogen with D212 and the SB because the CS of  $^{13}\text{C}\zeta$  in Y185 exhibits an even further down-field shift compared with the same carbon of Y57. Furthermore, the unusual up-field shift of the C14 resonance frequency of the Ret chromophore in both  $\text{bR}_{cis}$  and  $\text{bR}_{trans}$  can be attributed to the hydrophobic interaction with the aromatic ring of Y185. Cross-peaks of Y185C $\epsilon$ -RetC15 and Y185C $\zeta$ -RetC15 are not observed in  $\text{bR}_{cis}$ , indicating that the RetC15 could be more twisted and rigid than the other three  $^{13}\text{C}$ -labelled sites in  $\text{bR}_{cis}$ , and the Ret chromophore is relatively further from Y185 in  $\text{bR}_{cis}$  compared with  $\text{bR}_{trans}$ . This is supported by the chemical shifts, H–C–C–H torsion angles and H–C bond lengths

measurements here. The correlations between the other labelled sites with Ret and Y185 are difficult to resolve due to the significant overlap of the signals with the aromatic carbons from the 11 tyrosines.

Couplings of Y185 with the Ret chromophore in dark-adapted bR have been further studied by the direct mutagenesis. Figure 6 shows comparisons of the  $^{13}\text{C}$ – $^{13}\text{C}$  double-quantum filtration experimental results (Figure 6A) and the  $^{13}\text{C}$ – $^{13}\text{C}$  PDSD correlation experimental results (Figure 6B) on the wild-type and Y185F mutant bR incorporated with [10, 11, 14, 15- $^{13}\text{C}_4$ ]-Ret. The four carbon resonance assignments are listed in Table 2. Both down-field and up-field shifts are observed in the bR<sub>cis</sub> for the four carbon sites. There is no observable peak for the bR<sub>trans</sub> form in Y185F-bR. The *cis-trans* thermal isomerization equilibrium of the Ret chromophore is clearly shifted to a new position dominated by bR<sub>cis</sub>. The absorption maximum of 568 nm in the wild-type bR purple membrane shifts to 547.6 nm in the Y185F mutant (Table 3), which is similar to the result obtained for the bR membrane containing only the *cis* Ret previously [4, 31].

### 3.5 Coupling of Y185 with the proton release group in bR purple membranes

We further investigated the mediation mechanism of Y185 on the proton release group by a long-time molecular dynamic (MD) simulation and light-induced transient absorption change spectroscopy. Figure 7A shows the H-bond network around the D85-D212-R82 cluster in the bR crystal structure [48]. As shown, D212 is H-bonded with both Y185 through the phenolic hydroxyl group and the guanidine group of R82, bridged by a water molecule to maintain its conformation in the inactive state. However, a 1  $\mu\text{s}$  MD simulation shows that the guanidine group of R82

swings upwards by approximately 3 Å, and this distance may be sufficiently small to form a direct H-bond with D212 in the Y185F mutant (Figure 7B). In the M state, the crystal structure shows that the guanidine group of R82 needs to rotate downwards to form H-bonds with E194 and E204 to maintain the conformation of the proton release group, and assist the proton release in pumping out of the extracellular side (Figure 7C) [2]. However, to establish the H-bond network with E194 and E204, to maintain the conformation of the proton release group, and assist the proton release out of the extracellular side, R82 needs to swing down over a long distance of more than 9 Å in the Y185F mutant, as indicated by the MD simulation (Figure 7D). All results indicate that large conformational changes may be required during proton translocation at different intermediates in the Y185F mutant.

Figure 8 shows the transient absorption changes in the M state, O state and the recovery trajectory towards the bR ground state in the wild-type bR purple membrane (A-C) and Y185F mutant (E-G) at 410 nm, 660 nm and 570 nm, respectively. The proton pumping activities of the wild-type and Y185F mutant are shown in Figure 8D and 8H. Removal of the phenolic hydroxyl group in the Y185F mutant is seen to cause a weakening of the M state, loss of the O state and elongation of the recovery time and the proton pumping cycle time.

## **4. Discussion**

### **4.1 Mediation mechanism of Y185 on isomerization and binding of the retinal chromophore**

Solid-state NMR (ssNMR) has been extensively used to study various aspects of bR from the photocycle to different intermediates [56, 57]. Chemical shifts of the Ret

chromophore with singly  $^{13}\text{C}$  labelled at many positions along the polyene chain were measured in the bR purple membrane of dark-adapted, light-adapted and different photo intermediates [6, 58-63]. The H–C14–C15–H torsion angles in the light-adapted and the early and late M intermediates of the bR membrane were also determined [54]; moreover, a distortion around the C14–C15 bond in the light-adapted form, which was even more twisted in the M state, was observed [54].

By combining 2D heteronuclear and homonuclear correlation experiments, the chemical shifts of Y185 and of the Ret are resolved for most of the resonance sites in the purple membrane. Spectral line splitting was not observed for any of the resolved peaks of Y185 in the 2D NCOCX experiments, including  $^{13}\text{CO}$ ,  $^{13}\text{C}\alpha$ ,  $^{13}\text{C}\beta$ ,  $^{13}\text{C}\epsilon$  and  $^{13}\text{C}\zeta$ , as shown in Figure 2, which clearly indicates that Y185 maintains a single conformation in the dark-adapted bR purple membrane and further indicates that there is most likely no perturbation by the nearby residues in the binding pocket, including the *cis*–*trans* thermal conversion of Ret. The difference between this study and the work by others may be attributed to the different experiments used [25], with direct polarization transfer through a 2D scheme providing a less ambiguous result, whereas the results here are consistent with the crystal and solution NMR structures of  $\text{bR}_{\text{trans}}$  and  $\text{bR}_{\text{cis}}$  [27-29].  $\text{C}\zeta$  of Y185 shows a 2.2 ppm down-field shift compared with  $\text{C}\zeta$  of Y57, indicating a differential electrostatic interaction with Y185.  $\text{C}\epsilon$  of Y185 shows a 1.0 ppm up-field shift compared with  $\text{C}\epsilon$  of Y57, indicating a more hydrophobic local environment. The down-field shift of C15 in  $\text{bR}_{\text{cis}}$  and the larger peak separation between C15 and C14 in  $\text{bR}_{\text{cis}}$  than in  $\text{bR}_{\text{trans}}$  indicate that the C15–C14 bond may be more twisted in  $\text{bR}_{\text{cis}}$  or



that some extra interactions may occur at this site because the charge accumulation on the N–H bond of SB is likely similar in both the  $bR_{cis}$  and  $bR_{trans}$  forms.

Distortion of the C14–C15 bond in  $bR_{cis}$  is much more severe than that in the  $bR_{trans}$  configuration. The librational motion of each C–H bond remains quite similar, except for that of the C15–H bond in the  $bR_{cis}$  configuration, which shows unusual rigidity. This feature may indicate that the more populated  $bR_{cis}$  in the thermal equilibrium is stabilized by an interaction at the C15 site, likely the electrostatic interaction with the phenolic hydroxyl group of Y185, as indicated by the further down-field shift of the  $^{13}C\zeta$  chemical shift of Y185 in  $bR_{cis}$ . Distortion of the C14–C15 bond was previously observed in the light-adapted bR membrane, and the authors suggest that the protons of the C14-C15 moiety are twisted out of the plane of the chromophore, although the possibility that the heavy atoms of the  $bR_{trans}$  chromophore remain in-plane cannot be excluded [54]. Y185 holds a single configuration in the dark-adapted bR purple membrane. This stable configuration may be attributed to the hydrogen bonding of the phenolic hydroxyl hydrogen with D212 and the SB because the chemical shift of  $^{13}C\zeta$  in Y185 exhibits an even further down-field shift compared with the same carbon of Y57. The unusual up-field shift of the C14 resonance frequency of the Ret chromophore in both  $bR_{cis}$  and  $bR_{trans}$  can be attributed to the hydrophobic interaction with the aromatic ring of Y185. Cross-peaks of Y185C $\epsilon$ -RetC15 and Y185C $\zeta$ -RetC15 are not observed in  $bR_{cis}$ , indicating that the RetC15 could be more twisted and rigid than the other three  $^{13}C$ -labelled sites in  $bR_{cis}$ , and the Ret chromophore is relatively farther from Y185 in  $bR_{cis}$  compared with  $bR_{trans}$ . A much smaller separation between C11 and C10 may indicate that the C11–C10 bond remains relatively flat and less affected by the isomerization in both  $bR_{cis}$

and bR<sub>trans</sub>. Similar chemical shift values have been reported on singly C11-, C14- and C15-labelled Ret in dark-adapted bR purple membranes [53, 54].

Distortion of the C14–C15 bond has also been observed in light-adapted Proteorhodopsin [64], Anabaena Sensory Rhodopsin [65] and Channelrhodopsin-2 [66], indicating that the mediation of Y185 to the isomerization and binding of the Ret chromophore might be a common mechanism in bacterial rhodopsins, particularly those that are proton pumps.

#### **4.2 Mediation mechanism of Y185 on the H-bonding network around D85-D212-R82 in proton pumping channel**

Here, we report the first evidence that Y185 not only mediates the isomerization and binding of the Ret chromophore, but also mediates the H-bonding network around D85-D212-R82 in the proton pumping channel. Removal of the phenolic hydroxyl group in the Y185F mutant causes the guanidine group of R82 to swing upwards by approximately 3 Å from MD to form a direct H-bond with D212 to stabilize its conformation in the inactive state, which in turn weakens the formation of the M state. Removal of the phenolic hydroxyl group in the Y185F mutant further affects the H-bonding network along the proton pumping channel. The crystal structure shows that the guanidine group of R82 needs to rotate downwards to form H-bonds with E194 and E204 to maintain the conformation for the proton release out of the extracellular side in the M state [2]. However, this rotation needs to swing over a much longer distance to establish the H-bond network with E194 and E204 to maintain the conformation required for proton release, and assist the proton release for the Y185F mutant. More time is required to cover a longer distance, which

implies a weak formation and decay of the M state in the Y185F mutant. According to the crystal structure of 1JV7, the Ret chromophore is in the all-*trans* configuration in the O state [67]. The loss of the O state, as indicated by the measurement of light-induced transient absorption change spectroscopy (Figure 8), suggests that the all-*trans* Ret is missing; this absence is a direct consequence of the removal of the phenolic hydroxyl group in the Y185F mutant, as indicated here by the ssNMR and UV-vis measurements. These results prove that the 13-*cis* configuration is the main form in the Y185F mutant; therefore, the recovery time and proton pumping cycle time clearly increase in the absence of the H-bond.

Similar phenomena have been observed for different mutations in bR and other bacterial rhodopsins. Kouyama *et al.* reported that the M145F mutation in bR reduced the freedom of movement of the tryptophan 182 in contact with the C13 methyl group of the Ret and further destabilized the L state [19]. The dark state of Gloeobacter Rhodopsin (GR) contains primarily all-*trans* Ret both in its alkaline and acidic forms and does not show appreciable signs of dark or light adaptation; however, replacement of E132Q has been shown to lead to a dramatic increase in the 13-*cis* content of the dark state [68].

It is noteworthy that structural studies performed by X-ray diffraction and resonance Raman spectroscopy have shown that the Ret chromophore in Proteorhodopsin [10], Anabaena Sensory Rhodopsin [11] and Channelrhodopsin-2 [12] all maintain *cis-trans* thermal equilibrium in the inactive state. However, other structural studies conducted by ssNMR only show a single all-*trans* Ret chromophore in the protein inactive state of Proteorhodopsin [64], Anabaena Sensory Rhodopsin [65] and Channelrhodopsin-2 [66]. A structural comparison of the bR<sub>cis</sub> and bR<sub>trans</sub>

shows that Ret isomerization around the C13=C14 and the C15=N bonds is accompanied by noticeable displacements of a few residues in the vicinity of the Ret Schiff base and small rearrangement of the hydrogen-bonding network in the proton release channel, which indicates that variation in the structural rigidity within the Ret binding pocket is one of the important factors ensuring the stereospecific isomerization of Ret [27]. The tightly packed binding pocket can only accommodate the all-*trans* Ret but not the *cis* isomer, which may indicate less protein dynamics, a rigid environment and different photochemical reaction kinetics. It has been reported that although the general conclusions drawn from studies of bR mutants expressed in both *E. coli* and *H. salinarum* are similar regarding several of the important amino acid residues, the detailed results obtained for these two different systems have often varied [69]. It is clear that a native membrane lipid environment is very crucial to the transmembrane protein to maintain correct conformational dynamics to perform its complete dynamic function.

## 5. Conclusions

In summary, the experiments presented here demonstrate that the aromatic ring of Y185 plays an essential role in maintaining the twisted polyene chain of the Ret chromophore and stabilizing the *cis-trans* thermal equilibrium in the bR inactive state through electrostatic and hydrophobic interactions. Additionally, the removal of the phenolic hydroxyl group in the Y185F mutant causes a weakening of the M state, loss of the O state and elongation of the proton pump cycle time. This study establishes the basis for further investigations of the functional role of Y185 in the proton translocation mechanism of bR and the exploration of the possible existence

of coupling of the micro-switch in the protonation switch mechanism in the activation of the bacterial rhodopsin family of proteins. Similar electromechanical coupling is likely to occur in receptors and proteins in which tyrosine is coupled through hydrogen bonding to promote conformational changes through metastable thermal equilibria [70, 71], as demonstrated in this study.

## **Acknowledgements**

This work has been supported by the National Natural Science Foundation of China (grant numbers 30970657 and 21475045), Shanghai Pujiang Program (grant number 09PJ1404300), and East China Normal University (grant numbers 79003A29, 79301207, 79301411, and 41500-515430-14100) to XZ; by the Medical Research Council and Engineering and Physical Sciences Research Council of UK and the State Administration of Foreign Experts Affairs of China through the High-end Foreign Experts Recruitment Program (GDW20123100086) to AW; and by the National Natural Science Foundation of China (grant numbers 21573217, 31370714, and 91430110) to GHL. The EPSRC 850MHz NMR facility is also acknowledged for facility access (AW).

## References

- [1] D. Oesterhelt, W. Stoeckenius, Rhodopsin-like protein from the purple membrane of halobacterium halobium, *Nat New Biol*, 233 (1971) 149-152.
- [2] H. Luecke, B. Schobert, H.T. Richter, J.P. Cartailler, J.K. Lanyi, Structural changes in bacteriorhodopsin during ion transport at 2 angstrom resolution, *Science*, 286 (1999) 255-260.
- [3] D. Oesterhelt, M. Meentzen, L. Schuhmann, Reversible dissociation of the purple complex in bacteriorhodopsin and identification of 13-cis and all-trans-retinal as its chromophores, *Eur. J. Biochem.*, 40 (1973) 453-463.
- [4] W. Sperling, P. Carl, C.N. Rafferty, N.A. Dencher, Photochemistry and dark equilibrium of retinal isomers and bacteriorhodopsin isomers, *Biophys. Struct. Mech.*, 3 (1977) 79-94.
- [5] W. Stoeckenius, R.H. Lozier, R.A. Bogomolni, Bacteriorhodopsin and the purple membrane of halobacteria, *Biochim. Biophys. Acta*, 505 (1979) 215-278.
- [6] G.S. Harbison, S.O. Smith, J.A. Pardo, C. Winkel, J. Lugtenburg, J. Herzfeld, R. Mathies, R.G. Griffin, Dark-adapted bacteriorhodopsin contains 13-cis, 15-syn and all-trans, 15-anti retinal schiff bases, *Proc. Natl. Acad. Sci. U.S.A.*, 81 (1984) 1706-1709.
- [7] P. Scherrer, M.K. Mathew, W. Sperling, W. Stoeckenius, Retinal isomer ratio in dark-adapted purple membrane and bacteriorhodopsin monomers, *Biochemistry*, 28 (1989) 829-834.
- [8] J.K. Lanyi, Bacteriorhodopsin, *Annu. Rev. Physiol.*, 66 (2004) 665-688.
- [9] M. Sumii, Y. Furutani, S.A. Waschuk, L.S. Brown, H. Kandori, Strongly hydrogen-bonded water molecule present near the retinal chromophore of leptosphaeria rhodopsin, the bacteriorhodopsin-like proton pump from a eukaryote, *Biochemistry*, 44 (2005) 15159-15166.
- [10] T. Friedrich, S. Geibel, R. Kalmbach, I. Chizhov, K. Ataka, J. Heberle, M. Engelhard, E. Bamberg, Proteorhodopsin is a light-driven proton pump with variable vectoriality, *J. Mol. Biol.*, 321 (2002) 821-838.
- [11] L. Vogeley, O.A. Sineshchikov, V.D. Trivedi, J. Sasaki, J.L. Spudich, H. Luecke, Anabaena sensory rhodopsin: A photochromic color sensor at 2.0 Å, *Science*, 306 (2004) 1390-1393.
- [12] M. Nack, I. Radu, C. Bamann, E. Bamberg, J. Heberle, The retinal structure of channelrhodopsin-2 assessed by resonance raman spectroscopy, *FEBS Lett.*, 583 (2009) 3676-3680.

- [13] G. Varo, L. Zimanyi, X. Fan, L. Sun, R. Needleman, J.K. Lanyi, Photocycle of halorhodopsin from halobacterium salinarium, *Biophys. J.*, 68 (1995) 2062-2072.
- [14] S.P. Balashov, E.S. Imasheva, V.A. Boichenko, J. Anton, J.M. Wang, J.K. Lanyi, Xanthorhodopsin: A proton pump with a light-harvesting carotenoid antenna, *Science*, 309 (2005) 2061-2064.
- [15] K. Ihara, T. Amemiya, Y. Miyashita, Y. Mukohata, Met-145 is a key residue in the dark adaptation of bacteriorhodopsin homologs, *Biophys. J.*, 67 (1994) 1187-1191.
- [16] K. Inoue, T. Tsukamoto, K. Shimono, Y. Suzuki, S. Miyauchi, S. Hayashi, H. Kandori, Y. Sudo, Converting a light-driven proton pump into a light-gated proton channel, *J. Am. Chem. Soc.*, 137 (2015) 3291-3299.
- [17] N. Enamil, K. Yoshimura, M. Murakami, H. Okumura, K. Hara, T. Kouyama, Crystal structures of archaerhodopsin-1 and-2: Common structural motif in archaeal light-driven proton pumps, *J. Mol. Biol.*, 358 (2006) 675-685.
- [18] R. Henderson, J.M. Baldwin, T.A. Ceska, F. Zemlin, E. Beckmann, K.H. Downing, Model for the structure of bacteriorhodopsin based on high-resolution electron cryo-microscopy, *J. Mol. Biol.*, 213 (1990) 899-929.
- [19] T. Kouyama, R. Fujii, S. Kanada, T. Nakanishi, S.K. Chan, M. Murakami, Structure of archaerhodopsin-2 at 1.8 Å resolution, *Acta Crystallogr D Biol Crystallogr*, 70 (2014) 2692-2701.
- [20] K.J. Rothschild, P. Roepe, P.L. Ahl, T.N. Earnest, R.A. Bogomolni, S.K. Das Gupta, C.M. Mulliken, J. Herzfeld, Evidence for a tyrosine protonation change during the primary phototransition of bacteriorhodopsin at low temperature, *Proc. Natl. Acad. Sci. U.S.A.*, 83 (1986) 347-351.
- [21] P.L. Ahl, L.J. Stern, D. Düring, T. Mogi, H.G. Khorana, K.J. Rothschild, Effects of amino acid substitutions in the f helix of bacteriorhodopsin. Low temperature ultraviolet/visible difference spectroscopy, *J. Biol. Chem.*, 263 (1988) 13594-13601.
- [22] M. Shibata, T. Tanimoto, H. Kandori, Water molecules in the schiff base region of bacteriorhodopsin, *J. Am. Chem. Soc.*, 125 (2003) 13312-13313.
- [23] K.J. Rothschild, Y.W. He, S. Sonar, T. Marti, H.G. Khorana, Vibrational spectroscopy of bacteriorhodopsin mutants. Evidence that thr-46 and thr-89 form part of a transient network of hydrogen bonds, *J. Biol. Chem.*, 267 (1992) 1615-1622.
- [24] J. Herzfeld, S.K. Das Gupta, M.R. Farrar, G.S. Harbison, A.E. McDermott, S.L. Pelletier, D.P. Raleigh, S.O. Smith, C. Winkel, J. Lugtenburg, R.G. Griffin, Solid-state <sup>13</sup>C nmr study of tyrosine protonation in dark-adapted bacteriorhodopsin, *Biochemistry*, 29 (1990) 5567-5574.

- [25] I. Kawamura, N. Kihara, M. Ohmine, K. Nishimura, S. Tuzi, H. Saito, A. Naito, Solid-state nmr studies of two backbone conformations at tyr185 as a function of retinal configurations in the dark, light, and pressure adapted bacteriorhodopsins, *J. Am. Chem. Soc.*, 129 (2007) 1016-1017.
- [26] I. Kawamura, M. Ohmine, J. Tanabe, S. Tuzi, H. Saito, A. Naito, Dynamic aspects of extracellular loop region as a proton release pathway of bacteriorhodopsin studied by relaxation time measurements by solid state nmr, *Biochim. Biophys. Acta*, 1768 (2007) 3090-3097.
- [27] T. Nishikawa, M. Murakami, T. Kouyama, Crystal structure of the 13-cis isomer of bacteriorhodopsin in the dark-adapted state, *J. Mol. Biol.*, 352 (2005) 319-328.
- [28] H. Patzelt, B. Simon, A. terLaak, B. Kessler, R. Kuhne, P. Schmieder, D. Oesterhelt, H. Oschkinat, The structures of the active center in dark-adapted bacteriorhodopsin by solution-state nmr spectroscopy, *Proc. Natl. Acad. Sci. U.S.A.*, 99 (2002) 9765-9770.
- [29] H. Patzelt, A.S. Ulrich, H. Egbringhoff, P. Dux, J. Ashurst, B. Simon, H. Oschkinat, D. Oesterhelt, Towards structural investigations on isotope labelled native bacteriorhodopsin in detergent micelles by solution-state nmr spectroscopy, *J. Biomol. NMR*, 10 (1997) 95-106.
- [30] M. Groesbeek, J. Lugtenburg, Synthesis of doubly and multiply isotopically labeled retinals, *Photochem. Photobiol.*, 56 (1992) 903-908.
- [31] D. Oesterhelt, W. Stoeckenius, Isolation of the cell membrane of halobacterium halobium and its fractionation into red and purple membrane, *Methods Enzymol.*, 31 (1974) 667.
- [32] M. Rehorek, M.P. Heyn, Binding of all-trans-retinal to the purple membrane. Evidence for cooperativity and determination of the extinction coefficient, *Biochemistry*, 18 (1979) 4977-4983.
- [33] S.L. Helgerson, S.L. Siemsen, E.A. Dratz, Enrichment of bacteriorhodopsin with isotopically labeled amino acids by biosynthetic incorporation in halobacterium halobium, *Can. J. Microbiol.*, 38 (1992) 1181-1185.
- [34] D. Oesterhelt, L. Schuhmann, Reconstitution of bacteriorhodopsin, *FEBS Lett.*, 44 (1974) 262-265.
- [35] J.G. Hu, B.Q. Sun, M. Bizounok, M.E. Hatcher, J.C. Lansing, J. Raap, P.J.E. Verdegem, J. Lugtenburg, R.G. Griffin, J. Herzfeld, Early and late m intermediates in the bacteriorhodopsin photocycle - a solid-state nmr study, *Biochemistry*, 37 (1998) 8088-8096.



- [36] Z. Cao, X. Ding, B. Peng, Y. Zhao, J. Ding, A. Watts, X. Zhao, Novel expression and characterization of a light driven proton pump archaerhodopsin 4 in a halobacterium salinarum strain, *Biochim. Biophys. Acta*, 1847 (2015) 390-398.
- [37] G. Metz, X. Wu, S.O. Smith, Ramped-amplitude cross polarization in magic angle spinning nmr, *J. Magn. Reson. A*, 110 (1994) 219-227.
- [38] A.E. Bennett, C.M. Rienstra, M. Auger, K.V. Lakshmi, R.G. Griffin, Heteronuclear decoupling in rotating solids, *J. Chem. Phys.*, 103 (1995) 6951-6958.
- [39] C.J. Dickson, L. Rosso, R.M. Betz, R.C. Walker, I.R. Gould, Gafflipid: A general amber force field for the accurate molecular dynamics simulation of phospholipid, *Soft Matter*, 8 (2012) 9617-9627.
- [40] M.J. Frisch, G.W. Trucks, H.B. Schlegel, G.E. Scuseria, M.A. Robb, J.R. Cheeseman, G. Scalmani, V. Barone, B. Mennucci, G.A. Petersson, H. Nakatsuji, M. Caricato, Li, X., Hratchian, H. P., Izmaylov, A. F., Bloino, J., Zheng, G., Sonnenberg, J. L., Hada, M., Ehara, M., Toyota, K., Fukuda, R., Hasegawa, J., Ishida, M., Nakajima, T., Honda, Y., Kitao, O., Nakai, H., Vreven, T., Montgomery Jr., J. A., Peralta, J. E., Ogliaro, F., Bearpark, M. J., Heyd, J., Brothers, E. N., Kudin, K. N., Staroverov, V. N., Kobayashi, R., Normand, J., Raghavachari, K., Rendell, A. P., Burant, J. C., Iyengar, S. S., Tomasi, J., Cossi, M., Rega, N., Millam, N. J., Klene, M., Knox, J. E., Cross, J. B., Bakken, V., Adamo, C., Jaramillo, J., Gomperts, R., Stratmann, R. E., Yazyev, O., Austin, A. J., Cammi, R., Pomelli, C., Ochterski, J. W., Martin, R. L., Morokuma, K., Zakrzewski, V. G., Voth, G. A., Salvador, P., Dannenberg, J. J., Dapprich, S., Daniels, A. D., Farkas, Ö., Foresman, J. B., Ortiz, J. V., Cioslowski, J., and Fox, D. J., *Gaussian 09 in*, Gaussian, Inc., Wallingford, CT, 2009.
- [41] C.I. Bayly, P. Cieplak, W. Cornell, P.A. Kollman, A well-behaved electrostatic potential based method using charge restraints for deriving atomic charges: The resp model, *J. Phys. Chem.*, 97 (1993) 10269-10280.
- [42] E. Tajkhorshid, J. Baudry, K. Schulten, S. Suhai, Molecular dynamics study of the nature and origin of retinal's twisted structure in bacteriorhodopsin, *Biophys. J.*, 78 (2000) 683-693.
- [43] S. Hayashi, I. Ohmine, Proton transfer in bacteriorhodopsin: Structure, excitation, ir spectra, and potential energy surface analyses by an ab initio qm/mm method, *J. Phys. Chem. B*, 104 (2000) 10678-10691.
- [44] B. Hess, C. Kutzner, D. van der Spoel, E. Lindahl, Gromacs 4: Algorithms for highly efficient, load-balanced, and scalable molecular simulation, *J. Chem. Theory Comput.*, 4 (2008) 435-447.
- [45] S. Nosé, A unified formulation of the constant temperature molecular dynamics methods, *J. Chem. Phys.*, 81 (1984) 511-519.
- [46] M. Parrinello, A. Rahman, Polymorphic transitions in single crystals: A new molecular dynamics method, *J. Appl. Phys.*, 52 (1981) 7182-7190.

- [47] T. Darden, D. York, L. Pedersen, Particle mesh ewald: An  $n \cdot \log(n)$  method for ewald sums in large systems, *J. Chem. Phys.*, 98 (1993) 10089-10092.
- [48] H. Luecke, B. Schobert, H.T. Richter, J.P. Cartailler, J.K. Lanyi, Structure of bacteriorhodopsin at 1.55 Å resolution, *J. Mol. Biol.*, 291 (1999) 899-911.
- [49] J. Schaefer, R.A. McKay, E.O. Stejskal, Double-cross-polarization nmr of solids, *J. Magn. Reson.*, 34 (1979) 443-447.
- [50] L.C. Shi, M.A.M. Ahmed, W.R. Zhang, G. Whited, L.S. Brown, V. Ladizhansky, Three-dimensional solid-state nmr study of a seven-helical integral membrane proton pump-structural insights, *J. Mol. Biol.*, 386 (2009) 1078-1093.
- [51] V.A. Higman, K. Varga, L. Aslimovska, P.J. Judge, L.J. Sperling, C.M. Rienstra, A. Watts, The conformation of bacteriorhodopsin loops in purple membranes resolved by solid-state mas nmr spectroscopy, *Angew. Chem. Int. Ed.*, 50 (2011) 8432-8435.
- [52] N.M. Szeverenyi, M.J. Sullivan, G.E. Maciel, Observation of spin exchange by two-dimensional fourier transform <sup>13</sup>C cross polarization-magic-angle spinning, *J. Magn. Reson.*, 47 (1982) 462-475.
- [53] V.S. Bajaj, M.L. Mak-Jurkauskas, M. Belenky, J. Herzfeld, R.G. Griffin, Functional and shunt states of bacteriorhodopsin resolved by 250 ghz dynamic nuclear polarization-enhanced solid-state nmr, *Proc. Natl. Acad. Sci. U.S.A.*, 106 (2009) 9244-9249.
- [54] J.C. Lansing, M. Hohwy, C.P. Jaroniec, A.F.L. Creemers, J. Lugtenburg, J. Herzfeld, R.G. Griffin, Chromophore distortions in the bacteriorhodopsin photocycle: Evolution of the h-c14-c15-h dihedral angle measured by solid-state nmr, *Biochemistry*, 41 (2002) 431-438.
- [55] E. Crocker, A.B. Patel, M. Eilers, S. Jayaraman, E. Getmanova, P.J. Reeves, M. Ziliox, H.G. Khorana, M. Sheves, S.O. Smith, Dipolar assisted rotational resonance nmr of tryptophan and tyrosine in rhodopsin, *J. Biomol. NMR*, 29 (2004) 11-20.
- [56] J. Herzfeld, J.C. Lansing, Magnetic resonance studies of the bacteriorhodopsin pump cycle, *Annu. Rev. Biophys. Biomol. Struct.*, 31 (2002) 73-95.
- [57] H. Saito, A. Naito, Nmr studies on fully hydrated membrane proteins, with emphasis on bacteriorhodopsin as a typical and prototype membrane protein, *Biochim. Biophys. Acta*, 1768 (2007) 3145-3161.
- [58] J.M. Griffiths, A.E. Bennett, M. Engelhard, F. Siebert, J. Raap, J. Lugtenburg, J. Herzfeld, R.G. Griffin, Structural investigation of the active site in bacteriorhodopsin: Geometric constraints on the roles of asp-85 and asp-212 in the proton-pumping mechanism from solid state nmr, *Biochemistry*, 39 (2000) 362-371.

- [59] K.V. Lakshmi, M.R. Farrar, J. Raap, J. Lugtenburg, R.G. Griffin, J. Herzfeld, Solid state  $^{13}\text{C}$  and  $^{15}\text{N}$  nmr investigations of the n intermediate of bacteriorhodopsin, *Biochemistry*, 33 (1994) 8853-8857.
- [60] S.O. Smith, H.J.M. de Groot, R. Gebhard, J.M. Courtin, J. Lugtenburg, J. Herzfeld, R.G. Griffin, Structure and protein environment of the retinal chromophore in light- and dark-adapted bacteriorhodopsin studied by solid-state nmr, *Biochemistry*, 28 (1989) 8897-8904.
- [61] S.O. Smith, J. Courtin, E. van den Berg, C. Winkel, J. Lugtenburg, J. Herzfeld, R.G. Griffin, Solid-state  $^{13}\text{C}$  nmr of the retinal chromophore in photointermediates of bacteriorhodopsin: Characterization of two forms of m, *Biochemistry*, 28 (1989) 237-243.
- [62] G.S. Harbison, S.O. Smith, J.A. Pardo, J.M. Courtin, J. Lugtenburg, J. Herzfeld, R.A. Mathies, R.G. Griffin, Solid-state  $^{13}\text{C}$  nmr detection of a perturbed 6-s-trans chromophore in bacteriorhodopsin, *Biochemistry*, 24 (1985) 6955-6962.
- [63] G.S. Harbison, S.O. Smith, J.A. Pardo, P.P.J. Mulder, J. Lugtenburg, J. Herzfeld, R. Mathies, R.G. Griffin, Solid-state  $^{13}\text{C}$  nmr studies of retinal in bacteriorhodopsin, *Biochemistry*, 23 (1984) 2662-2667.
- [64] J. Mao, N.-N. Do, F. Scholz, L. Reggie, M. Mehler, A. Lakatos, Y.-S. Ong, S.J. Ullrich, L.J. Brown, R.C.D. Brown, J. Becker-Baldus, J. Wachtveitl, C. Glaubitz, Structural basis of the green-blue color switching in proteorhodopsin as determined by nmr spectroscopy, *J. Am. Chem. Soc.*, 136 (2014) 17578-17590.
- [65] S. Wang, R.A. Munro, L. Shi, I. Kawamura, T. Okitsu, A. Wada, S.Y. Kim, K.H. Jung, L.S. Brown, V. Ladizhansky, Solid-state nmr spectroscopy structure determination of a lipid-embedded heptahelical membrane protein, *Nat. Methods*, 10 (2013) 1007-1012.
- [66] J. Becker-Baldus, C. Bamann, K. Saxena, H. Gustmann, L.J. Brown, R.C. Brown, C. Reiter, E. Bamberg, J. Wachtveitl, H. Schwalbe, C. Glaubitz, Enlightening the photoactive site of channelrhodopsin-2 by dnp-enhanced solid-state nmr spectroscopy, *Proc. Natl. Acad. Sci. U.S.A.*, 112 (2015) 9896-9901.
- [67] S. Rouhani, J.P. Cartailler, M.T. Facciotti, P. Walian, R. Needleman, J.K. Lanyi, R.M. Glaeser, H. Luecke, Crystal structure of the d85s mutant of bacteriorhodopsin: Model of an o-like photocycle intermediate, *J. Mol. Biol.*, 313 (2001) 615-628.
- [68] A.R. Choi, L. Shi, L.S. Brown, K.H. Jung, Cyanobacterial light-driven proton pump, *gloeobacter rhodopsin*: Complementarity between rhodopsin-based energy production and photosynthesis, *PLoS One*, 9 (2014) e110643.
- [69] L. Song, D.F. Yang, M.A. Elsayed, J.K. Lanyi, Retinal isomer composition in some bacteriorhodopsin mutants under light and dark-adaptation conditions, *J. Phys. Chem.*, 99 (1995) 10052-10055.

[70] R. Nygaard, T.M. Frimurer, B. Holst, M.M. Rosenkilde, T.W. Schwartz, Ligand binding and micro-switches in 7tm receptor structures, *Trends Pharmacol. Sci.*, 30 (2009) 249-259.

[71] A.Y.-H. Woo, K. Jozwiak, L. Toll, M.J. Tanga, J.A. Kozocas, L. Jimenez, Y. Huang, Y. Song, A. Plazinska, K. Pajak, R.K. Paul, M. Bernier, I.W. Wainer, R.-P. Xiao, Tyrosine 308 is necessary for ligand-directed gs protein-biased signaling of  $\beta$ 2-adrenoceptor, *J. Biol. Chem.*, 289 (2014) 19351-19363.

## Figure captions

**Figure 1.** Function assessments of the reconstituted purple membrane by UV-VIS measurements (A1-A3); formation and decay of the M state (B1-B3); and proton pumping behaviour (C1-C3) of the wild-type bR purple membrane before bleaching (A1, B1, C1), after bleaching (A2, B2, C2) and regenerated with the  $^{13}\text{C}$ -labelled retinal (A3, B3, C3). Clearly, the bR function was restored completely after reconstitution of the retinal.

**Figure 2.** 2D NCOCX spectra of the dark-adapted bR purple membrane with the selective labelling scheme of  $[\text{U-}^{13}\text{C}_9, ^{15}\text{N}]\text{-Y-}$ ,  $[\text{Y-}^{15}\text{N}]\text{-P-}$ , and  $[\text{Y-}^{15}\text{N}]\text{-L-}$ . CO (A),  $\text{C}\alpha\text{-C}\beta$  (B) and aromatic ring (C) regions with the peak assignments are shown.

**Figure 3.** 2D  $^{13}\text{C}\text{--}^{13}\text{C}$  PDS D correlation spectra of the dark-adapted bR purple membrane with fully  $^{13}\text{C}$ - and  $^{15}\text{N}$ -labelled tyrosine. The cross-peaks are shown in red for Y57 and blue for Y185.

**Figure 4.** 2D DQ-SQ correction spectra on  $[\text{10, 11, 14, 15-}^{13}\text{C}_4]\text{-Ret-}$ labelled bR purple membrane with four carbon resonance assignments. Projection of the acquisition dimension is shown above the 2D spectra to assist visualization. Colour coding, red:  $\text{bR}_{\text{trans}}$ ; blue:  $\text{bR}_{\text{cis}}$ .

**Figure 5.** 2D  $^{13}\text{C}$  PDS D spectra of the  $[\text{U-}^{13}\text{C}_9, ^{15}\text{N}]\text{-Y}$  and  $[\text{10, 11, 14, 15-}^{13}\text{C}_4]\text{-Ret-}$ labelled bR purple membrane. The cross-peak assignments are highlighted in blue for the correlations in  $\text{bR}_{\text{cis}}$  and red for the correlations in  $\text{bR}_{\text{trans}}$  between the aromatic ring of Y185 and the four labelled carbon sites of the Ret polyene chain.

**Figure 6.** 2D  $^{13}\text{C}$ – $^{13}\text{C}$  PDSD correlation spectra of the [10, 11, 14, 15- $^{13}\text{C}_4$ ]-Ret-labelled wild-type bR in the dark-adapted purple membrane (A); 2D  $^{13}\text{C}$ – $^{13}\text{C}$  PDSD correlation spectra of the [10, 11, 14, 15- $^{13}\text{C}_4$ ]-Ret-labelled Y185F mutant in the dark-adapted purple membrane.

**Figure 7.** Crystal structure of the region around Ret-D85-D212-R82 H-bonding network in the bR ground state (A); superposition of the WT-bR and Y185F-bR structures in the ground state (B); superposition of crystal structures of the ground state and M state (C); and superposition of the WT-bR and Y185F-bR structures in the M state (D).

**Figure 8.** Light-induced transient absorption changes in the spectra of the M state, O state and recovery trajectory to the ground state at 410 nm, 660 nm and 570 nm, and the net proton pumping activity, which is determined using the absorbance difference at 456 nm before and after adding the dye, respectively. A-D: WT-bR purple membrane, E-H: Y185F-bR mutant purple membrane.

## Tables

**Table 1.** Chemical shift assignments of Y185 and Y57 in the dark-adapted bR purple membrane

**Table 2.** Chemical shifts of [10, 11, 14, 15-<sup>13</sup>C<sub>4</sub>]-Ret labelled wild-type and Y185F mutant in the dark-adapted bR purple membrane

**Table 3.** Maximum UV-vis absorption of WT- and Y185F-bR in the purple membrane measured at room temperature

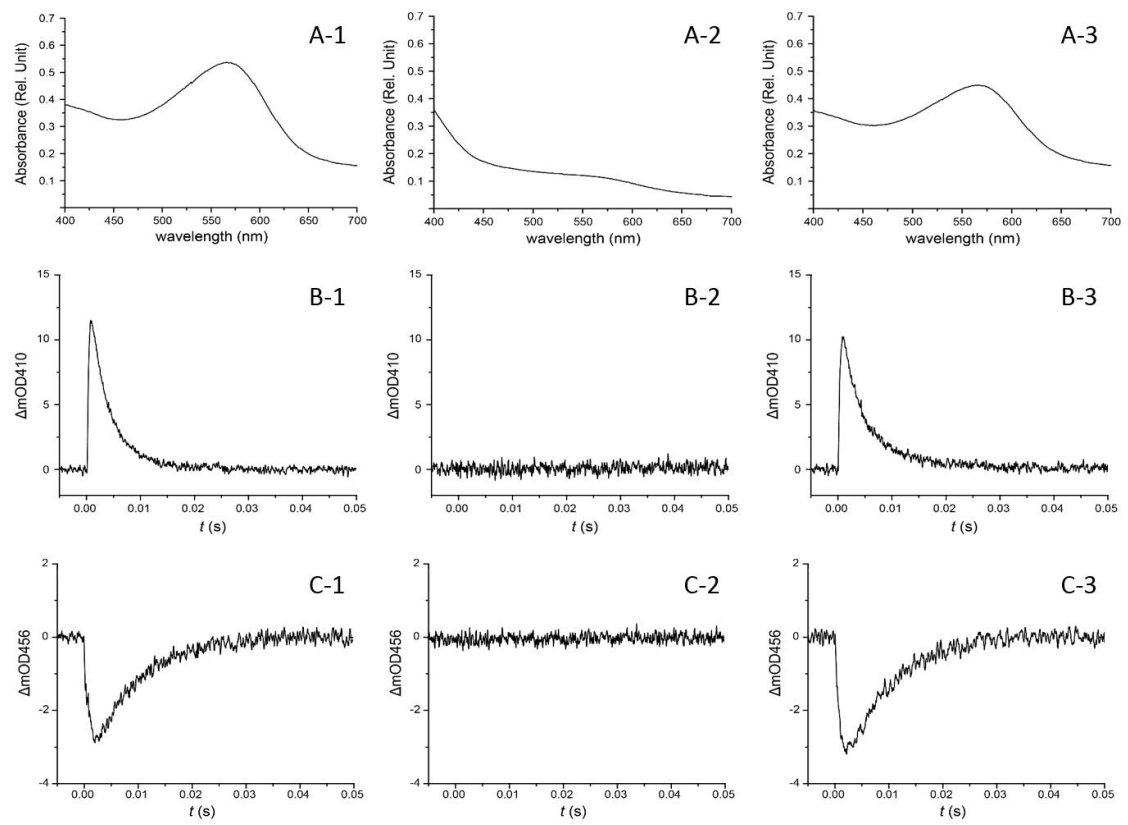


Figure 1



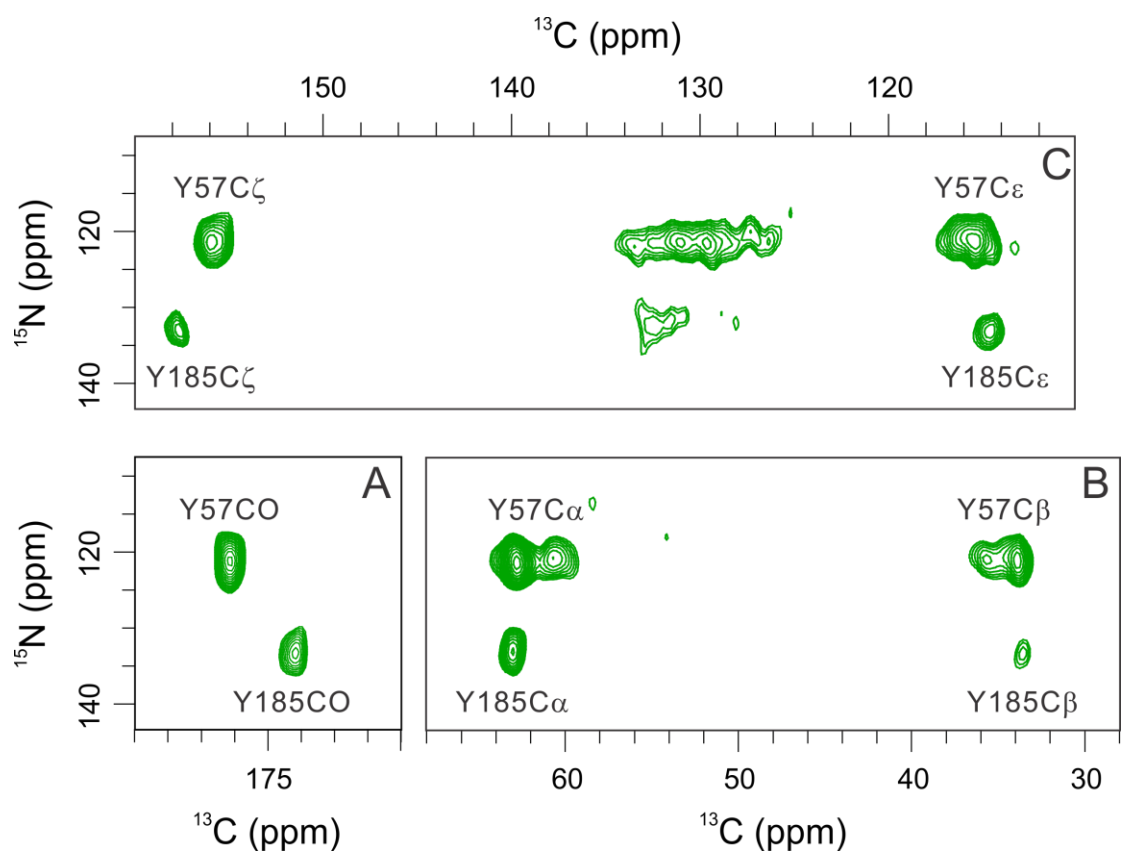
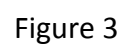


Figure 2



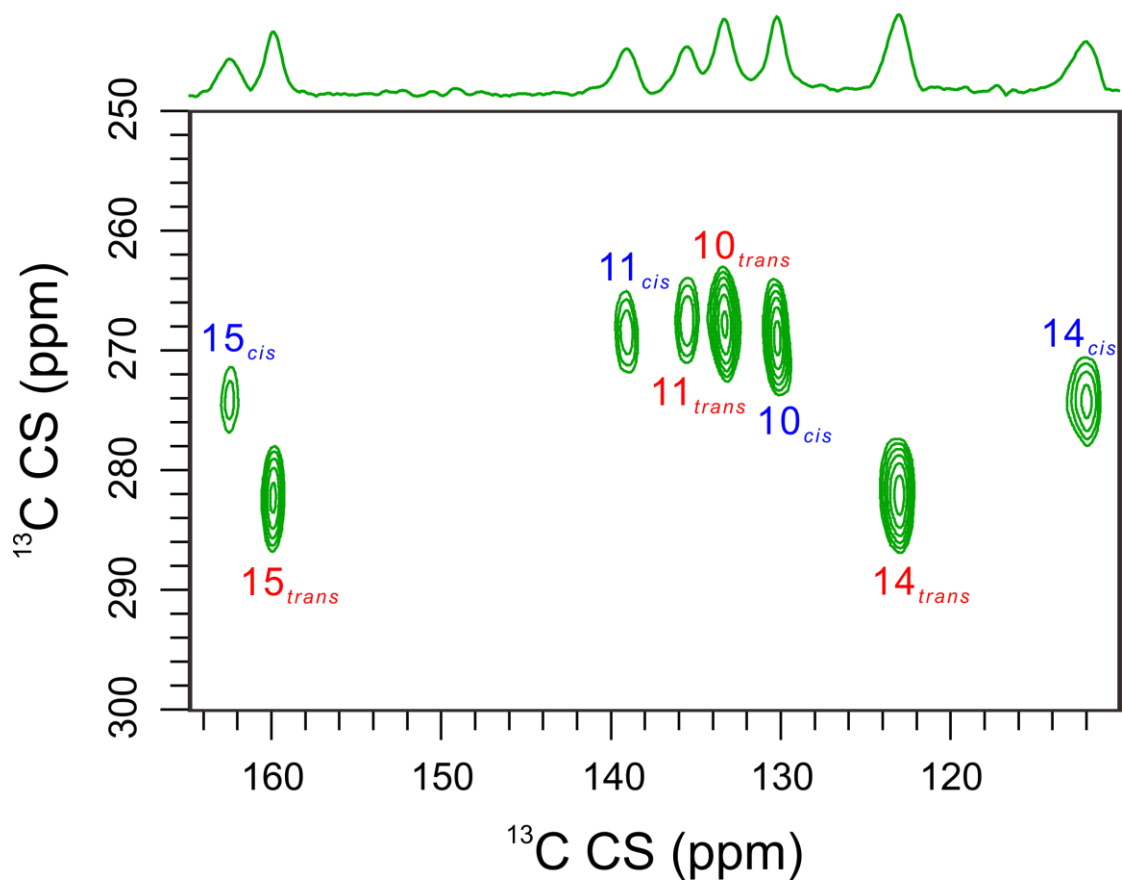


Figure 4

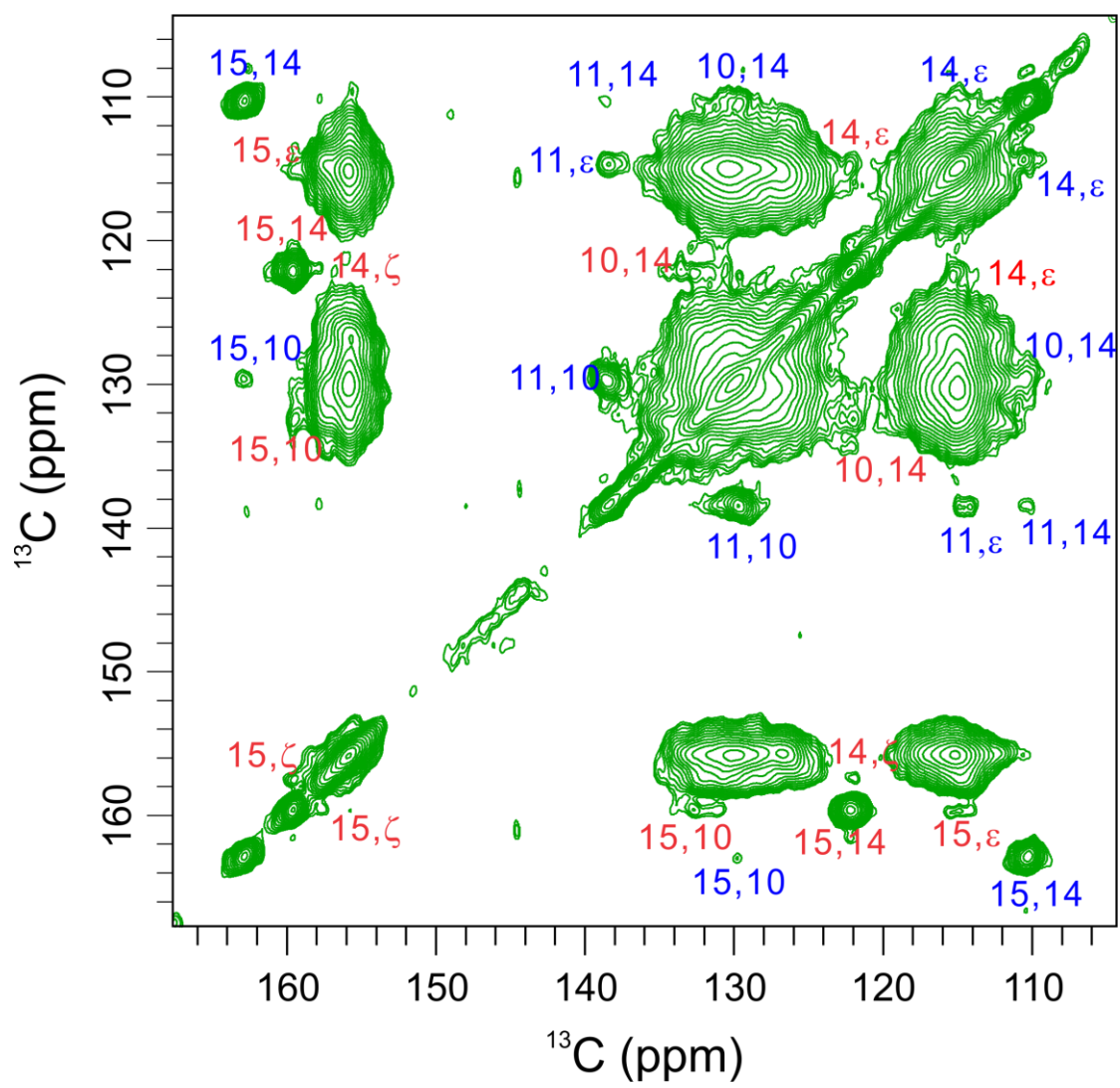


Figure 5

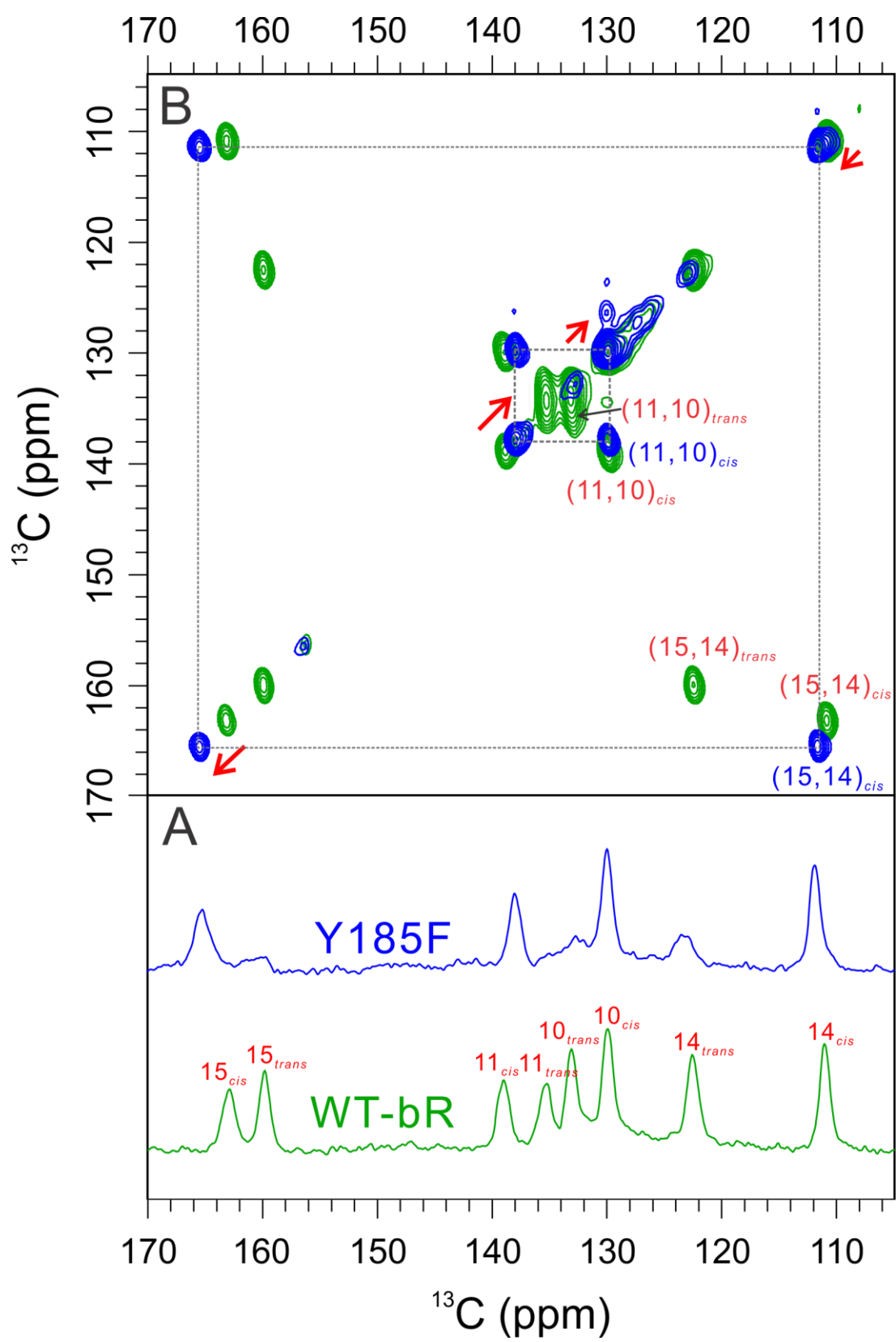


Figure 6

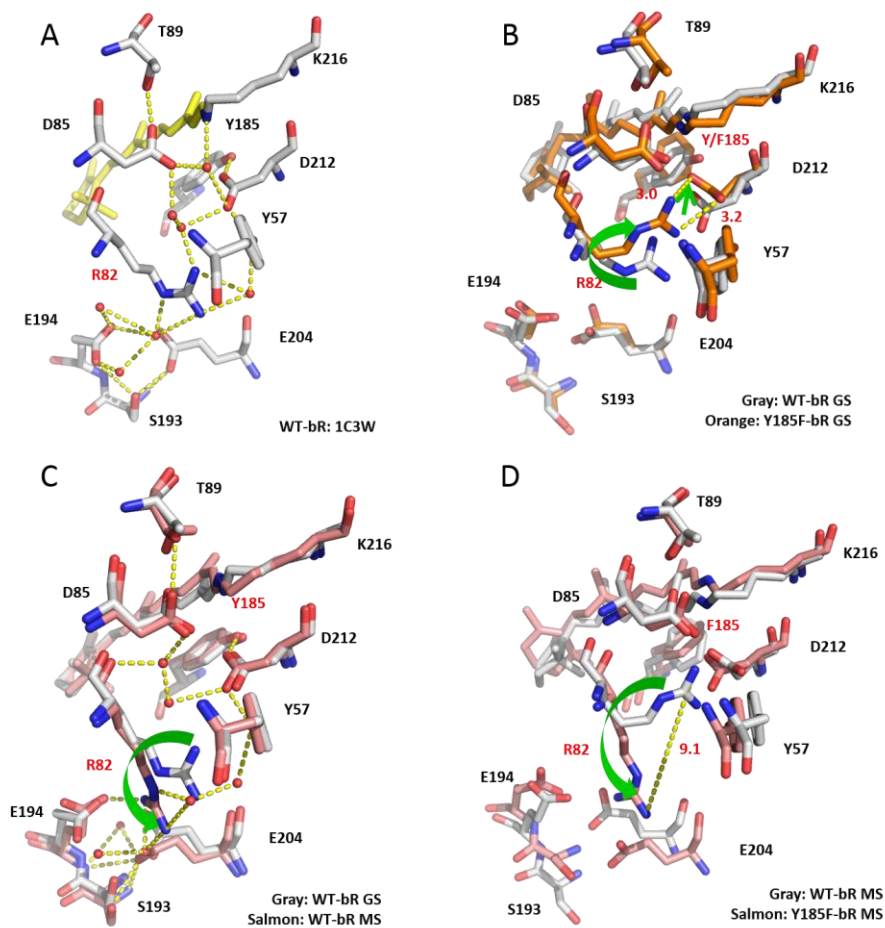


Figure 7

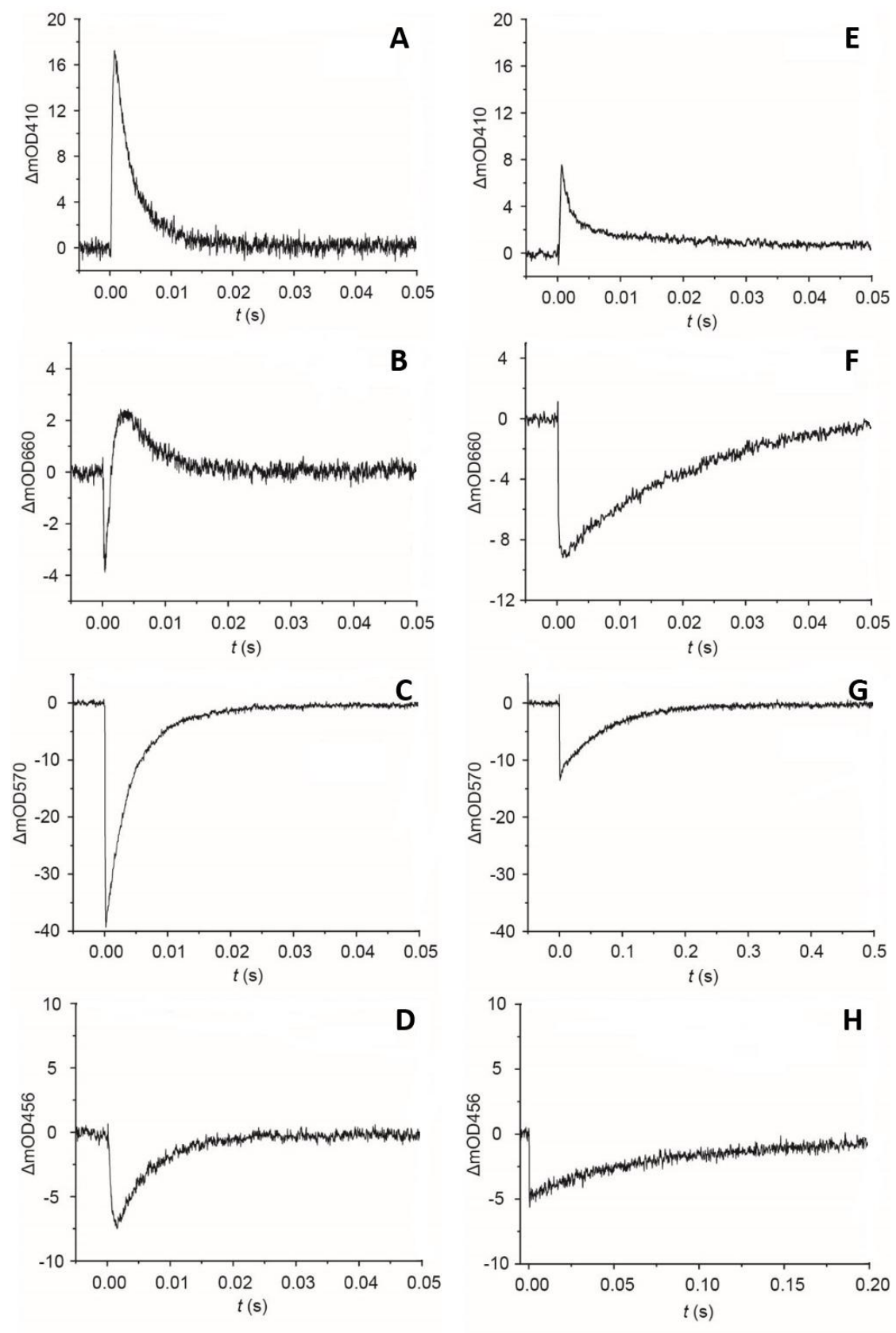


Figure 8

**Table 1.**

<b>Y185 (ppm)</b>						
CO	C $\alpha$	C $\beta$	C $\gamma$	C $\delta$	C $\epsilon$	C $\zeta$
174.2	63.1	33.6	128.4	132.8	115.3	158.0
<b>Y57 (ppm)</b>						
CO	C $\alpha$	C $\beta$	C $\gamma$	C $\delta$	C $\epsilon$	C $\zeta$
176.2	62.8	33.8	131.3	131.3	115.6	155.8



**Table 2.**

<b>WT-bR<sub>cis</sub></b>				<b>WT-bR<sub>trans</sub></b>			
C10	C11	C14	C15	C10	C11	C14	C15
130.0	139.0	111.0	163.2	133.2	135.4	122.7	160.0
<b>Y185F-bR<sub>cis</sub></b>				<b>Y185F-bR<sub>trans</sub></b>			
C10	C11	C14	C15	C10	C11	C14	C15
130.0	138.0	111.8	165.4	-	-	-	-



**Table 3.**

$\lambda$ (nm)	WT	Y185F	Ref
$\lambda_{R_{cis}}$	548		[4]
$\lambda_{R_{trans}}$	568		[4]
Dark-adapted	555		[4, 31]
	555.0	547.6	This work
Light-adapted	568		[4, 31]
	568.0	566.0	This work